Environmental Science and Pollution Research (2019) 26:8914–8927
https://doi.org/10.1007/s11356-019-04382-0

RESEARCH ARTICLE

Thermochemical degradation of furfural by sulfate radicals in aqueous solution: optimization and synergistic effect studies

Reza Shokoohi[1] · Somaye Bajalan[1] · Mehdi Salari[1] · Amir Shabanloo[1]

Received: 17 September 2018 / Accepted: 24 January 2019 / Published online: 4 February 2019

Abstract

In this study, thermochemical degradation of furfural by sulfate radical has been investigated to find the best-operating conditions. For this purpose, the response surface methodology (RSM) based on central composite design (CCD) was applied to optimize the five independent variables of thermally activated persulfate (TAP)/nZVI oxidation process including pH, PS concentration, furfural concentration, nZVI dosage, and heat. The ANOVA results ("$P > F$ value" < 0.0001 and R^2_{adj} = 0.9701) showed the obtained quadratic model is acceptable to predict furfural removal. Based on the reduced quadratic model PS concentration, nZVI dosage, and heat revealed the positive effects on removal efficiency, while pH and furfural concentration had a negative effect. Accordingly, 98.4% of furfural could be removed within 60 min of reaction under the optimum conditions: pH 5.26, PS concentration of 20.52 mM, furfural concentration of 84.32 mg/L, nZVI dosage of 1.15 mg/L, and a temperature of 79 °C. In such circumstances, the furfural removal efficiency for TAP, PS/nZVI, PS, and nZVI was 94.5, 9, 3, and 2%, respectively. Therefore, based on the synergy index (SI) values, the combination of PS, nZVI, and heat can lead to a synergistic effect in the performance of the thermochemical process.

Keywords Furfural · Thermally activated persulfate · Synergistic effect · Sulfate radical · Optimization · Central composite design

Introduction

Furfural, as an excellent organic solvent, is widely used in the oil and petroleum refining, pulp and paper, pharmaceutical, petrochemical, and food industries (He et al. 2014). Therefore, the effluent of these industries contains various concentrations of furfural. For instance, the furfural concentration in the Pars oil refinery wastewater is reported as 100–2000 ppm (Jafarinejad 2017). Also, the furfural concentration in raw wastewater of furfural manufacturing industry can reach to at least 600 mg/L (Wirtz and Dague 1993). Furfural, known as a toxic and non-biodegradable substance in aquatic ecosystems, causes health concerns for human life (Borghei and Hosseini 2008). For example, if furfural is accidentally ingested, it will cause death, as well as its dermal absorption will cause acute damage to the nervous system and the lungs (Cuevas et al. 2014). Liver enlargement, the feeling of weakness, skin rash, tremor, and nose bleeding are also the long-term (chronic) effects of exposure to furfural (Nezamzadeh-Ejhieh and Moeinirad 2011). Today, a variety of different physicochemical methods, including adsorption (Sahu et al. 2008; Singh et al. 2009), photocatalytic oxidation (Faramarzpour et al. 2009), membrane technology (Wang et al. 2018a), and biological treatment (Zhang et al. 2013), have been investigated for furfural removal. However, due to high temperature (98 °C) of the raw wastewater of furfural manufacturing industry (Wirtz and Dague 1993), commercialization of conventional methods will not be easy (Veisi et al. 2016). Generally, the biological process is a time-consuming and costly approach (He et al. 2014), and activated carbon as the most common adsorbent only transfers the pollutant from

Responsible editor: Ioannis A. Katsoyiannis

✉ Amir Shabanloo
shabanlo_a@yahoo.com

Reza Shokoohi
reza.shokohi@umsha.ac.ir

Somaye Bajalan
s72.bajalan@yahoo.com

Mehdi Salari
msalari_22@yahoo.com

[1] Department of Environmental Health Engineering, School of Health, Hamadan University of Medical Sciences, Hamadan, Iran

the liquid to the solid phase and its regeneration cost is very high (Purkait et al. 2007). Recently, sulfate radical-based advanced oxidation processes ($SO_4^{\bullet-}$ -AOP$_s$) have been introduced as a promising method for degradation of resistant organic contaminants (Hu and Long 2016). $SO_4^{\bullet-}$ radicals can be generated through activation process of the persulfate anion ($S_2O_8^{2-}$ -PS) (2.01 V). The homogeneous transition metal ions (Me^{2+}), US radiation (Seid-Mohammadi et al. 2017), UV (Lin et al. 2011), heat (Frontistis et al. 2017), and electrochemical process (Rahmani et al. 2016; Song et al. 2018) are often used for this purpose. Among these methods, the use of heat-activated PS or thermally activated persulfate (TAP) oxidation process has attracted considerable attention as an attractive and clean method for the degradation of numerous organic contaminants (Nie et al. 2014).

According to the studies, $SO_4^{\bullet-}$ -AOP$_s$ have more advantages compared to $OH^{\bullet}$-AOP$_s$, including (i) $SO_4^{\bullet-}$ (2.5–3.1 V) in contrast to $OH^{\bullet}$ (acidic pH = 2.4–2.7 V, alkaline pH = 1.9–2.0 V) has a higher redox potential (Ferkous et al. 2017), (ii) the half-life period of $SO_4^{\bullet-}$ (3–4 × 10 s) is generally more than $OH^{\bullet}$ (2 × 10 s) (Olmez-Hanci and Arslan-Alaton 2013), (iii) the oxidation potential of the $OH^{\bullet}$ decreases significantly at alkaline pH, whereas $SO_4^{\bullet-}$ can oxidize the pollutants effectively over a wide pH range (Hu and Long 2016), and (iv) $SO_4^{\bullet-}$ is more selective than $OH^{\bullet}$ for degradation of contaminants (Deng et al. 2013). The use of binary or ternary PS activation techniques due to synergistic effect can reduce the energy consumption and increase the process efficiency (Chakma et al. 2017). In this regard, nZVI can be a good permanent source of Fe^{2+} to continuously release iron for activation of PS (Dong et al. 2017). Eq. (1) shows the TAP oxidation process (Frontistis et al. 2017; Zarei et al. 2015), Eqs. (2) and (3) describe the reaction between the PS and nZVI particles (Wang et al. 2014), and Eq. (4) demonstrate the activation of PS by Fe^{2+} (Rahmani et al. 2017).

$$S_2O_8^{2-} \xrightarrow{heat} 2SO_4^{-} \quad \left(30^{\circ}C < T < 99^{\circ}C\right) \tag{1}$$

$$Fe^0 + H^+ \rightarrow Fe^{2+} + H_2 \quad \text{(Acidic conditions)} \tag{2}$$

$$Fe^0 + S_2O_8^{2-} \rightarrow Fe^{2+} + 2SO_4^{2-} \tag{3}$$

$$Fe^{2+} + S_2O_8^{2-} \rightarrow Fe^{3+} + SO_4^{\bullet-} + SO_4^{2-} \tag{4}$$

Based on the literatures review and authors' knowledge, no study has been done to optimize and identify the synergy effect of thermochemical degradation of furfural. Therefore, in this study, $SO_4^{\bullet-}$ radicals were generated using TAP/nZVI (binary PS activation) process, then the most effective operational parameters were optimized by RSM based on the CCD. After optimizing the process, the synergistic effect among PS, nZVI, and heat was investigated.

Materials and methods

Chemicals

Furfural (99%), sodium persulfate (≥ 99%), ferrous heptahydrate sulfate (≥ 98%), and sodium borohydride (≥ 98%) were procured from Sigma Company. Sodium hydroxide pellet (NaOH), sulfuric acid (98%), starch, and ethanol were procured from Merck company. A number of the most important physicochemical characteristics of furfural are given in Table 1.

Experimental setup and procedure

The experiments were carried out in a batch rectangular cube Plexiglass reactor with the working volume of 4500 mL. In order to prevent evaporation of furfural from the samples, the reactor was equipped to a reflux condenser. Adjustment of the solution temperature at desired levels was conducted by a water heater element (Jupiter, 2000 W–220 V, number and length of legs were 2 and 30 cm, respectively) equipped with a thermostat. An air pump (7 W–220 V, air flow and pressure were 3000 mL/min, and 0.015 MPa, respectively) was used to ensure sufficient mixing and uniformity of the reactor temperature. The schematic of the experimental setup is shown in Fig. 1. About 0.44 mL of furfural solution was dissolved in 1000 mL of deionized water to prepare the stock solution of 500 mg/L concentration, then other studied concentrations were provided by dilution of the stock solution. After reaching to the intended temperature, a known amount of nZVI and PS was introduced into the sample solution, based on the experimental design. Then pH of the resulting solution was adjusted at the designed values using H_2SO_4 and NaOH (pH meter; SensION, HACH). At the end of 60-min thermochemical reaction, 10 mL of the solution was taken and the furfural concentration was measured at the maximum wavelength (λ_{max} = 275 nm) using UV–Vis spectrophotometer (DR5000, HACH) (Lucas et al. 2004; Sahu et al. 2007). The mineralization of furfural was determined by vario TOC cube (Elementar Analysensysteme GmbH, Germany) TOC analyzer. The nZVI particles were prepared by sodium borohydride ($NaBH_4$) reduction method (Babuponnusami and Muthukumar 2012) and characterized using transmission electron microscopy (TEM) analysis (EM208S, Philips).

Experimental design

Different studies have been done to optimize and investigate the effect of independent variables and their interactions using RSM based on CCD (Cho and Zoh 2007; Hazime et al. 2013; Zarei et al. 2015). In this study, the RSM-CCD was applied to optimize of thermochemical degradation of furfural. Therefore, the initial pH of the solution, PS and furfural

Table 1 Physicochemical characteristics of furfural

Chemical structure	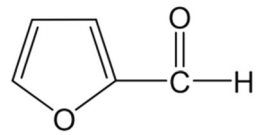	(Nezamzadeh-Ejhieh and Moeinirad 2011)
Chemical formula	$C_5H_4O_2$	
pH	5	
λ_{max}	254 nm	
Color	Light brown	
Molecular weight	96.082 g/mol	(Zeitsch 2000)
Boiling point (760 mmHg)	161.7 °C	
Freezing point	− 36.5 °C	
Ignition temperature	315 °C	
Flash point (closed cup)	59 °C	
Specific gravity	1.16 g/cm	
Solubility in water at 20 °C	8.3 g/100 mL of water	

concentration, nZVI dosage, and solution temperature were investigated as independent variables at five levels ($-\alpha$, -1, 0, $+1$, $+\alpha$), while furfural removal efficiency was considered as response factor. The five independent variables and their coded levels are shown in Table 2. The ranges of variables were chosen based on pre-test and literatures review. Finally, a total of 50 experiment runs were designed based on CCD, as illustrated in Table 3. In this study, the number of independent variables is five ($i = 5$), so the CCD consists of 32 factorial runs, 10 axial runs, and 8 replicates at the central points (C), as calculated from Eq. (5) (Anupam et al. 2011; Cho and Zoh 2007; Eslami et al. 2016).

$$\text{Number of runs} = 2^{i} + 2i + c = 2^{5} + (2 \times 5) + 8 = 50 \quad (5)$$

The experimental design and data analysis were conducted by the statistical software of design expert, version 11.0.0. The validation of the predicted model, as well as the relationship between independent variables and response factor, was analyzed through the analysis of variance (ANOVA). Also, the interaction of independent variables was investigated using 3D plots.

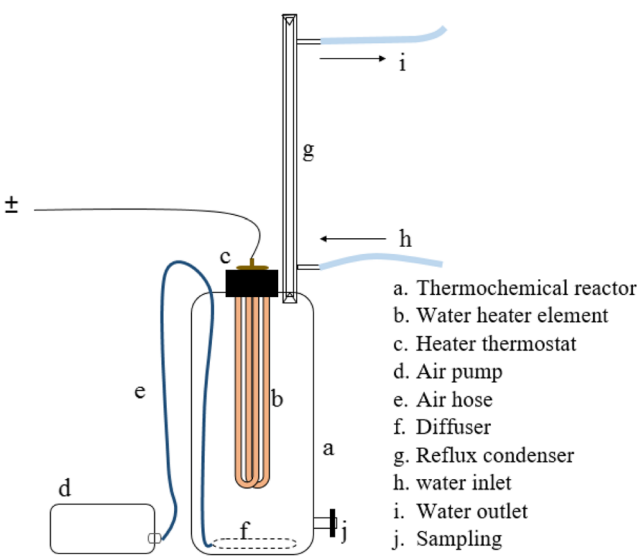

Fig. 1 The schematic of TAP reactor

Synergy index calculation

In optimal condition, the synergetic effect among PS, nZVI, and heat was calculated using the pseudo-first-order degradation rate constants (K_{obs}), according to Eq. (6) (Durán et al. 2016). In this equation, SI values smaller or greater than 0 illustrate an antagonistic or synergistic effect between the components, respectively. While SI values equal to 0 demonstrate an additive effect.

$$\mathrm{SI} = \frac{K_T - (K_1 + K_2 + \cdots + K_n)}{K_T} \quad (6)$$

where K_T is the pseudo-first-order degradation rate constant of hybrid processes (TAP/nZVI, TAP, and PS/nZVI) and K_1, K_2, and K_n are the constants of separate processes (PS, heat, and nZVI).

Results and discussion

TEM analysis

Figure 2 depicted the TEM image of the synthesized nZVI particles. As can be seen, the synthesized particles are at the nano-scale with the average size about 20–100 nm (Yehia et al. 2015). According to the result of TEM, the nZVI particles were almost in a smooth spherical shape with a core-shell structure (Liu et al. 2015), so that the Fe^0 nanoparticles were encapsulated by the iron oxide shell (Vilardi et al. 2018).

Table 2 The five independent variables and their levels ($\alpha = 2$)

Variables	Unit	Symbols	Coded levels				
			$-\alpha$ Factorial points	-1 Axial points	0 Center point	$+1$ Axial points	$+\alpha$ Factorial points
pH	–	A	3	5	7	9	11
PS concentration	mM	B	5	10	15	20	25
Furfural concentration	mg/L	C	25	50	75	100	125
nZVI dosage	mg/L	D	0.5	1	1.5	2	2.5
Heat (temperature)	°C	E	40	50	60	70	80

The experiments design and data analysis

The results of the actual and predicted furfural removal efficiency are shown in Table 3. According to the fit summary analysis, the quadratic model was suggested as the most robust model to predict the response. The validity evaluation of the proposed model to predict the response factor was performed by analysis of variance (ANOVA). The results of ANOVA are presented in Table 4.

The values of P value lees than 0.0500 indicate that the model terms are significant, while the terms with the greater values of that were removed from the model. Accordingly, in this study A, B, C, D, E, CE, A^2, B^2 were the significant model terms. The reduced quadratic model to predict the furfural removal efficiency based on the actual factors has been illustrated in Eq. (7).

$$X = -93.21 + 3.58\,A + 1.93\,B + 0.37\,C + 2.77\,D + 2.42\,E - 0.0091\,CE - 0.327A^2 - 0.05B^2 \quad (7)$$

In this equation, X is the predicted furfural removal efficiency as well as A, B, C, D, and E are independent variables, as defined in Table 2. As well as the Pareto chart was used to examine the contribution of each independent variable in the removal of furfural (Abdessalem et al. 2008). According to Eq. (8), the Pareto effect (P_i) was calculated based on the coded factors as displayed in the Fig. 3.

$$P_i\,(\%) = \left[\frac{(b_i^2)}{\sum b_i^2}\right] \times 100 \quad (i \neq 0) \quad (8)$$

where b_i represents the regression coefficient of each term in accordance with coded values. As seen from Fig. 3, the contribution of each term is different in the process, where the highest effect in first-order terms has been assigned to the heat. Also, the blue and red colors show the positive and negative effects of independent variables on the furfural removal efficiency, respectively (Moghaddam et al. 2010).

According to the ANOVA results, the model F value of 199.83 and $P > F$ value less than 0.0001 indicate that the proposed quadratic model is significant (Priya et al. 2018). For the Lack of fit, the F value was obtained to be 2.54, which means that it is not significant relative to the experimental error, so the model is fitted as well (Moradi et al. 2016). The validity and accuracy of the obtained quadratic model can be guaranteed by a suitable R^2 value. In this way, the closer coefficients to 1 indicate more favorable conditions (Ghafari et al. 2009). Also, if R^2 and adjusted R^2 $\left(R^2_{adj}\right)$ are close together, it means that there are no unnecessary variables in the model (Asfaram et al. 2016). According to Table 4, in this study, the values of R^2 and R^2_{adj} are 0.9750 and 0.9701, respectively. The Adeq Precision term is defined as the signal to noise ratio and the value greater than 4 will be desirable for the model. In this study, the signal to noise ratio is 56.417, so the signal of the model is adequate (Sharma et al. 2017). The ratio of standard error of estimate to the mean value of observed response defines as coefficient of variance (CV). This coefficient shows the repeatability power of the proposed model. In general, if the CV is less than 10%, the model is repeatable (Ghafari et al. 2009). Considering the value of CV (4.27%), it can be concluded that the proposed model has a desirable repeatability.

To determine the adequacy of the model, diagnostic plots were used. The difference between the experimental values from the predicted values by the model is called the residual. Accordingly, for diagnosis of data normality, the normal probability plot of the studentized residuals was used.

As shown in Fig. 4 a, all the experimental values are located approximately on the central line, indicating that the data is normalized in the model prediction (Cho and Zoh 2007; Eslami et al. 2016).

Figure 4 b shows the actual values versus the predicted response by model. It is observed that the experimental results were in excellent correlation with the values predicted, which indicates the suitability of the model (Moradi and Ghanbari 2014).

Table 3 Experimental design and the value of actual and predicted furfural removal efficiency

Run	Coded levels of variables					Removal %	
	A	B	C	D	E	Actual value	Predicted value
1	9	10	50	1	50	45.5	46.85
2	5	10	100	2	50	46	49.58
3	7	15	75	1.5	60	69.5	70.27
4	5	20	100	1	50	49.5	50.88
5	5	20	50	2	50	56.5	57.69
6	7	25	75	1.5	60	73.5	69.25
7	9	20	50	1	70	92.5	90.35
8	9	20	100	2	70	80.2	79.98
9	5	20	100	2	70	83.5	83.98
10	7	15	25	1.5	60	78	78.86
11	7	15	75	1.5	80	97.5	100
12	5	20	100	2	50	49.3	53.65
13	9	10	100	2	50	44.5	45.58
14	5	10	100	1	70	75.5	77.14
15	7	15	75	1.5	60	69.1	70.27
16	9	10	50	2	50	48.5	49.62
17	7	15	125	1.5	60	62.5	61.68
18	5	10	50	2	50	53	53.62
19	7	5	75	1.5	60	60.5	61.11
20	9	10	100	1	50	42.2	42.81
21	5	20	100	1	70	80.5	81.21
22	7	15	75	1.5	60	75	70.27
23	9	10	50	2	70	89.2	89.05
24	11	15	75	1.5	60	60.2	61.03
25	9	20	50	2	70	95.5	93.12
26	5	10	50	2	70	94.5	93.05
27	7	15	75	1.5	60	70.5	70.27
28	5	10	50	1	70	89.5	90.28
29	3	15	75	1.5	60	73.5	69.03
30	7	15	75	2.5	60	75.8	73.04
31	9	20	50	2	50	52.5	53.69
32	7	15	75	1.5	60	70.2	70.27
33	9	20	100	1	50	44.5	46.88
34	5	20	50	1	50	55	54.92
35	9	20	100	2	50	46.5	49.65
36	5	10	100	1	50	50.2	46.81
37	5	20	50	1	70	93.2	94.35
38	9	10	100	1	70	75.8	73.14
39	9	10	100	2	70	77.4	75.91
40	7	15	75	1.5	40	45	35.39
41	5	20	50	2	70	97.5	97.12
42	5	10	100	2	70	80.2	79.91
43	7	15	75	1.5	60	68.9	70.27
44	5	10	50	1	50	48.5	50.85
45	9	10	50	1	70	87.5	86.28
46	7	15	75	1.5	60	70.8	70.27
47	7	15	75	1.5	60	71.1	70.27
48	9	20	100	1	70	79.5	77.21
49	7	15	75	0.5	60	67.2	67.5
50	9	20	50	1	50	47.2	50.92

The effect of independent variables on furfural removal efficiency

The effect of PS concentration

Based on the obtained quadratic model, the effect of independent variables as well as their interaction on the prediction of furfural removal efficiency was investigated using 3D response surface plots, as shown in Fig. 5.

Accordingly, the interaction of PS concentration and pH on furfural removal efficiency is shown in Fig. 5 a. As can be seen, PS concentration variations can affect the removal efficiency in this way that the removal efficiency continuously increased with increasing of PS concentration from 5 to 20 mM. However, with increasing PS concentrations from 20 to 25 mM, the removal efficiency decreased. Increasing the PS concentration as the only source of $SO_4^{\bullet-}$ radicals (Eq. 1) can enhance the removal efficiency (Liu et al. 2018; Nie et al. 2014). However, it has been reported that with increasing PS from a certain concentration, the removal efficiency will be reduced due to self-scavenging of $SO_4^{\bullet-}$ radicals according to Eq. (9). This scavenging reaction can also occur between $SO_4^{\bullet-}$ radicals and high concentrations of PS, as shown in Eq. (10). These undesirable reactions will consume both PS and radicals and subsequently, the removal efficiency will be reduced. In this regard, similar results have been reported in degradation of penicillin G by heat-activated persulfate (Norzaee et al. 2018), and

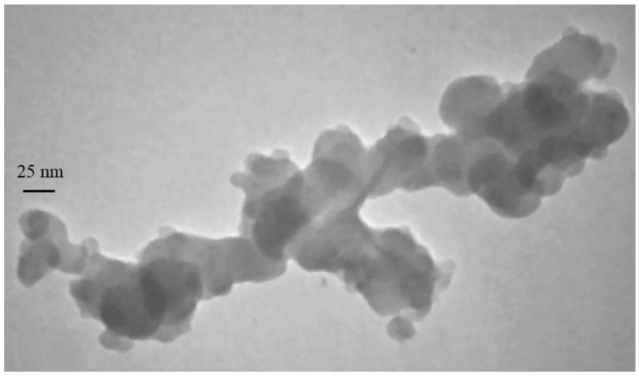

Fig. 2 TEM image of synthesized nZVI

Table 4 ANOVA results of the reduced quadratic model for the furfural removal efficiency

Source	Sum of squares	Degrees of freedom	Mean square	*F* value	Probability, *P* (*P* > *F* value)
Model	13578.96	8	1697.37	199.83	< 0.0001
A-pH	160	1	160	18.84	< 0.0001
B-PS	165.65	1	165.65	19.5	< 0.0001
C-furfural	737.88	1	737.88	86.87	< 0.0001
D-nZVI	76.73	1	76.73	9.03	0.0045
E-heat	12166.14	1	12166.14	1432.31	< 0.0001
CE	165.62	1	165.62	19.5	< 0.0001
A	55.02	1	55.02	6.48	0.0148
B	51.92	1	51.92	6.11	0.0177
Residual	348.26	41	8.49		
Lack of fit	322.1	34	9.47	2.54	0.101
Pure error	26.16	7	3.74		
Corrected total	13927.22	49			
$R^2 = 0.975$					
Adjusted $R^2 = 0.9701$					
Adequate precision = 56.417					
C.V. (%) = 4.27					

the treatment of dinitrodiazophenol industrial wastewater in heat-activated persulfate system (Wei et al. 2018).

$$SO_4^{\bullet-} + SO_4^{\bullet-} \rightarrow S_2O_8^{2-} \quad (9)$$

$$S_2O_8^{2} + SO_4^{\bullet-} \rightarrow S_2O_8^{\bullet-} + SO_4^{2-} \quad (10)$$

The effect of pH

As seen in Fig. 5 a, the highest furfural removal efficiency was observed at pH 5–6. In PS-based oxidation process, the pH variations can have a significant effect on the contaminant removal efficiency (Cai et al. 2018). Liang and Su (2009) found that the pH can affect the dominant radical species at heat-activated PS system, and the results of their study are summarized in Fig. 6. According to Eqs. (11) and (12), $SO_4^{\bullet-}$ in acidic solution can be easily formed through the acid-catalyzation reaction. In this condition, the $SO_4^{\bullet-}$ has the highest oxidation potential. As a result, furfural removal efficiency will increase (Ji et al. 2016).

However, in alkaline solution (pH > 8.5), $SO_4^{\bullet-}$ and OH^- react and produce $OH^\bullet$ radical as shown in Eq. (13) (Huang et al. 2002; Nie et al. 2014). Since the oxidation potential and lifetime of the $OH^\bullet$ radical decreases significantly under alkaline conditions, the removal efficiency decreases even in the presence of this radical (George et al. 2001; Lau et al. 2007). With further increase in pH, especially pH > 12, the reaction

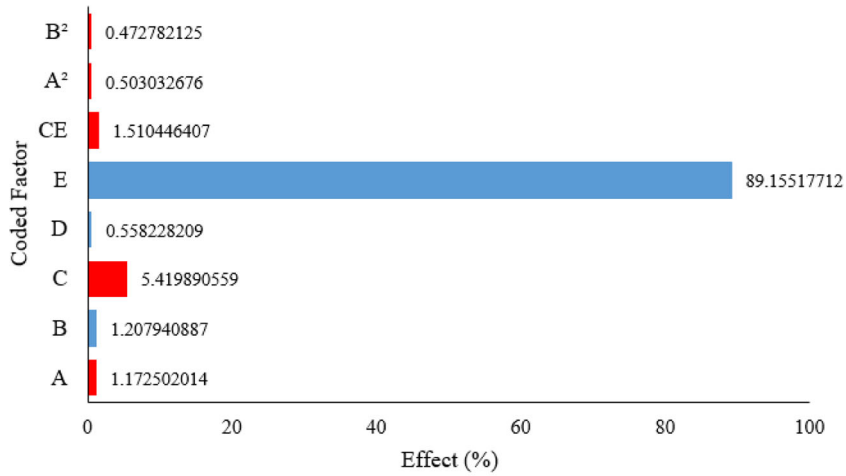

Fig. 3. Pareto chart (■ negative effect, ■ positive effect)

Fig. 3 Pareto chart (red, negative effect; blue, positive effect)

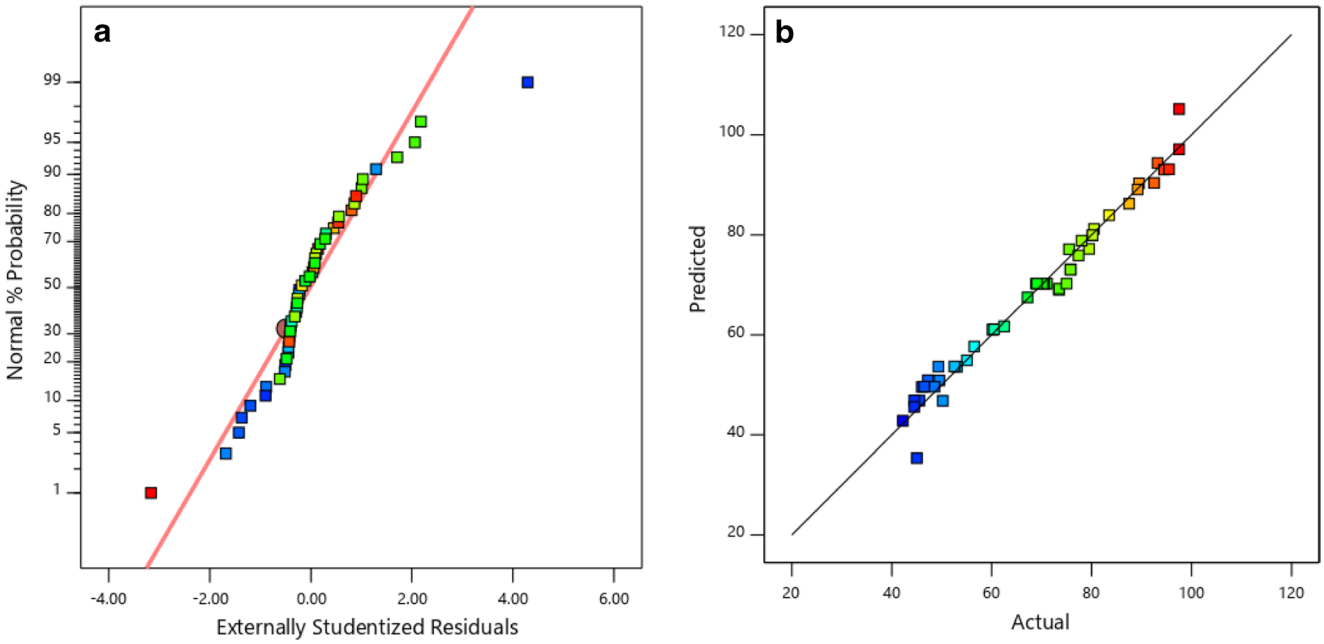

Fig. 4 Normal plot of residuals (**a**), predicted vs actual plots (**b**)

between $SO_4^{\bullet-}$ and $OH^{\bullet}$ radicals (Eq. 14), as well as scavenging of $OH^{\bullet}$ radicals by OH^- (Eq. 15) will lead to radical elimination from the oxidation system (Khan et al. 2017; Rani et al. 2009). For these reasons, the lowest furfural removal efficiency was obtained at pH 11.

$$S_2O_8^{2-} + H^+ \rightarrow 2HS_2O_8^- \quad (11)$$

$$HS_2O_8^- + \rightarrow SO_4^{\bullet-} + SO_4^{2-} + H^+ \quad (12)$$

$$SO_4^{\bullet-} + OH^- \rightarrow SO_4^{2-} + OH^{\bullet} \quad (13)$$

$$SO_4^{\bullet-} + OH^{\bullet} \rightarrow HSO_4^- + \frac{1}{2}O_2 \quad (14)$$

$$OH^{\bullet} + OH^- \rightarrow O^- + H_2O \quad (15)$$

Ghauch et al. (2012) obtained the maximum ibuprofen removal efficiency at pH 4. Liu et al. (2018) also found that the best degradation of sulfachloropyridazine (SCP) achieved at the acidic condition of reaction solution.

The effect of temperature

Figure 5 b illustrates the effect of variations of heat and furfural concentration on the prediction of removal efficiency. As can be seen, with increasing heat, the removal efficiency is drastically increased. So that, at the optimum concentration of furfural (see Fig. 8), the predicted removal efficiency at temperatures of 40, 50, 60, 70, and 80 °C was obtained 33.5, 52,65, 82, and 100%, respectively. According to Eq. (1), higher temperatures provide more energy to cleavage the O–O bands of PS anions, as a result, the furfural removal efficiency will increase continuously with increasing temperature (Gao et al. 2015). Similar results have been reported in accordance with our findings, for example, degradation of p-nitrophenol in TAP process (Chen et al. 2016), oxidation of indomethacin in the thermo-activated peroxydisulfate system (Li et al. 2018), and oxidation of cefalexin by TAP (Qian et al. 2018).

To calculate the PS activation energy at temperatures of 40–80 °C, the furfural removal efficiency was investigated at the reaction time of 0 to 60 min. The results of this section of the study are shown in Fig. 7. As illustrated in Figs. 7 a and b, the furfural degradation was well fitted with the pseudo-first-order kinetic model. The furfural degradation pseudo-first-order rate constant (k_{obs}) can be calculated from Eq. (16) (Ji et al. 2015).

$$\ln\left(\frac{[\text{furfural}]_t}{[\text{furfural}]_0}\right) = -k_{obs} \times \text{time} \quad (16)$$

Figure 7 c shows that with increasing of reaction temperature, the K_{obs} greatly increased. Therefore, based on the temperature–K_{obs} dependence, the energy required for PS activation was calculated from the Arrhenius equation (Eqs. 17, 18, and 19) (Zhao et al. 2014).

$$\ln K_{obs} = \ln A - \left(\frac{E_a}{RT}\right) \quad (17)$$

$$\ln K_{obs} = -\left(\frac{E_a}{R}\right)\left(\frac{1}{T}\right) + \ln A \quad (18)$$

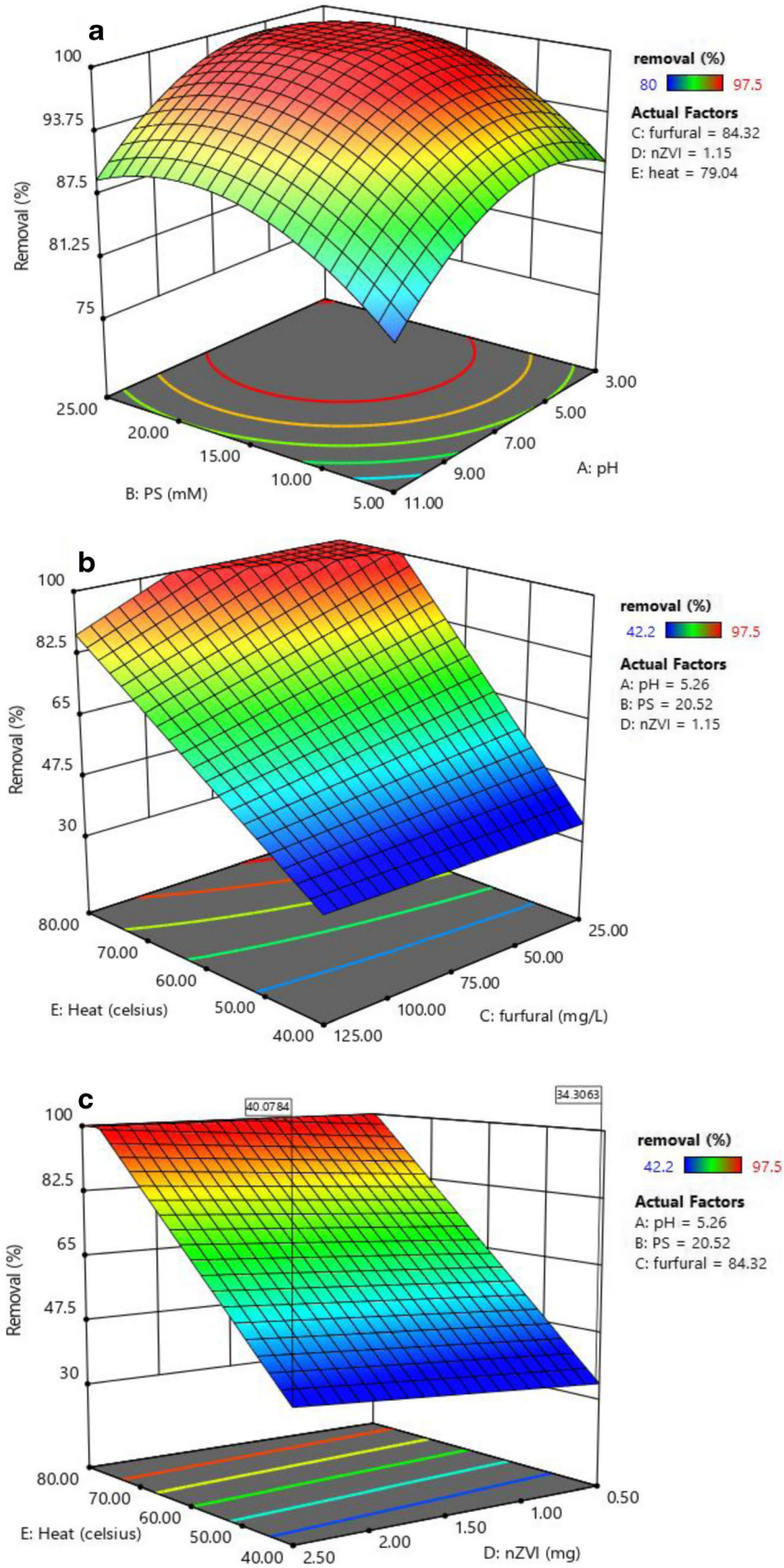

Fig. 5 3D plots for prediction of furfural removal efficiency (%) at optimal conditions ($\alpha = \pm 2$): The interaction of PS-pH (**a**), the interaction of heat-furfural (**b**), and the interaction of heat-nZVI (**c**)

$$E_a = -(\text{the slope of Arrhenius equation}) \times R \quad (19)$$

where A is the pre-exponential factor, E_a is the apparent PS activation energy (J mol), R is the ideal gas constant (8.314 J mol K), and T is the reaction temperature (k). Accordingly, based on the obtained equation from Fig. 7 d (Eq. 20), the E_a was determined to be 40.84 kJ mol (Eq. 21), which is much less than the values reported in previous studies (Ji et al. 2015; Liu et al. 2018; Norzaee et al. 2018).

$$\ln(K_{obs}) = -(-4911{\cdot}7)\left(\frac{1}{T}\right) + 10{\cdot}832 \quad (R = 0.9837) \quad (20)$$

$$E_a = -(-4911{\cdot}7) \times 8{\cdot}314 = 40835{\cdot}87\,\text{J}{\cdot}\text{mol}^{-1} \quad (21)$$

The effect of furfural concentration

The effect of different furfural concentrations on the TAP/nZVI oxidation process efficiency was also shown in Fig. 5b. As the results show, at 70 °C, by increasing the furfural concentration from 25 to 125 mg/L, the predicted furfural removal efficiency decreases from 100 to 71.5%. At a constant PS concentration (20.52 mM), the increase of furfural concentrations led to the decrease of $\frac{[SO_4^{\bullet-}]}{[\text{furfural}]}$ ratios (Tan et al. 2015). Also by increasing furfural concentration, degradation of byproducts derived from that increases during the process. These intermediate compounds can consume both $SO_4^{\bullet-}$ and $OH^{\bullet}$ radicals. Therefore, the $\frac{[SO_4^{\bullet-}]}{[\text{furfural}]}$ ratio will decrease further and as a result, the process efficiency will be reduced (Wang et al. 2018b).

The effect of nZVI dosage

Figure 5 c illustrates the influence exerted by nZVI concentration on furfural removal efficiency. At a constant temperature of 40 °C, it is quite clear that as nZVI increased from 0.5 to 2.5 mg/L, the predicted furfural removal efficiency increase from 34.3 to 40%. According to Eqs. (2), (3), and (4), by increasing the nZVI dosage, the number of active sites for Fe release will increase. Consequently, more $SO_4^{\bullet-}$ radicals will be generated, improving the removal efficiency (Gao et al. 2018; Hussain et al. 2012; Oh et al. 2009).

Process optimization

In order to obtain the highest furfural removal efficiency, the effective operating parameters must be optimized. For this purpose, optimization was performed based on the proposed model (Eq. 7). In this way, the desired goal for independent variables was adjusted at "in range" mode with the importance of 3, while furfural removal efficiency as the response factor was adjusted at the "maximize" mode (equal to 100%) with the importance of 5. Finally, one solution (desirability = 1.000) was selected as the optimal condition. The output of optimal conditions for the TAP/nZVI process is shown in Fig. 8. To evaluate the accuracy of the model prediction, a supernumerary experiment was performed at three replications in the optimized values. Subsequently, the experimental removal efficiency was obtained to be 98.4%, which was nearly consistent with the model's predicted response (100%). Therefore, the accuracy of the proposed model can be proved.

The identification of synergistic effect

In order to obtain the furfural removal efficiency under different reaction system as a function of time, the performance of non-activated PS, nZVI, heat, PS/nZVI, PS/heat (TAP), and TAP/nZVI systems were investigated at optimal condition. Figure 9 a shows the removal efficiency of furfural under different systems. As can be seen, after 60 min of reaction, the furfural removal efficiency for PS and nZVI alone was between 2 and 3%, as well as sole heat had a negligible

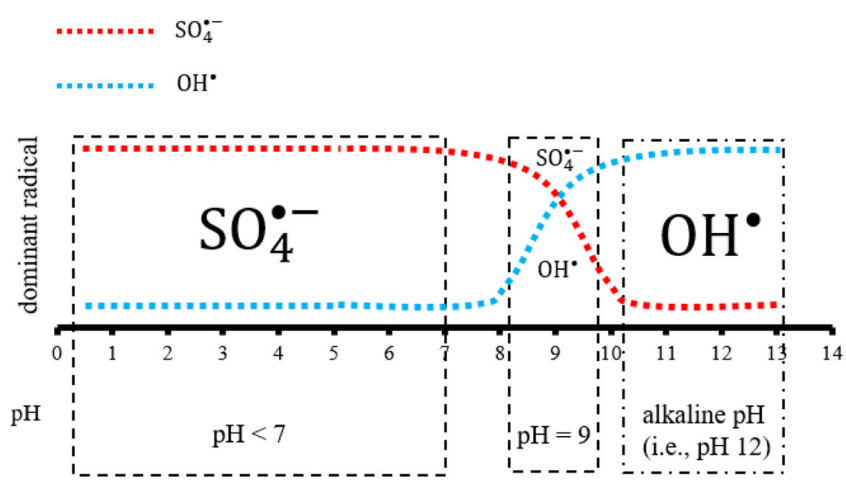

Fig. 6 The effect of pH on the dominant radical species at TAP oxidation process

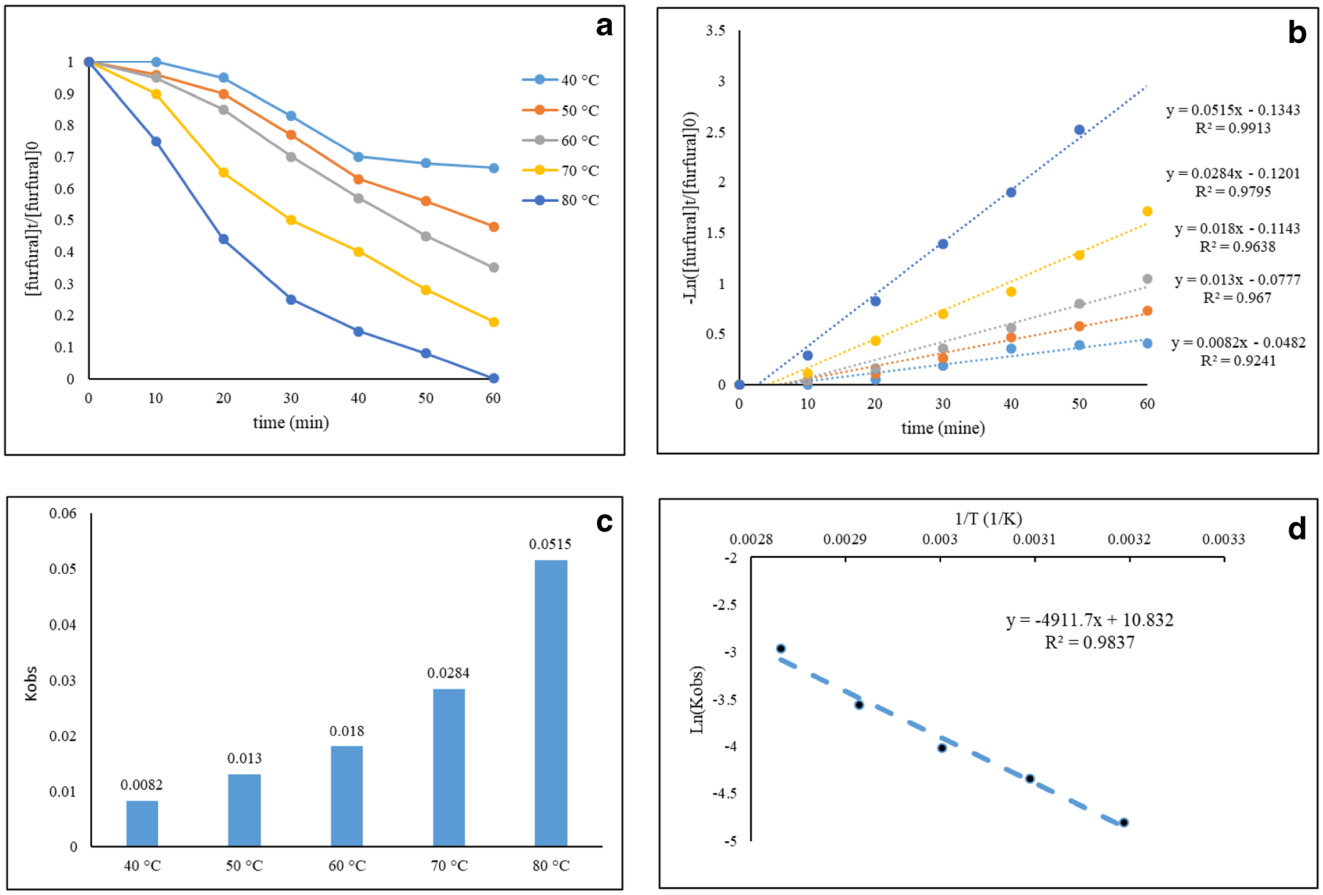

Fig. 7 The effect of TAP temperatures on furfural degradation (**a**). The pseudo-first-order kinetic reaction equations derived from **a** (**b**). The pseudo-first-order rate constants under different temperatures derived from **b** (**c**). The Arrhenius plot for E_a estimation (**d**). (pH = 5.26, $[\text{furfural}]_0$ = 84.3 mg/L, nZVI = 1.15 mg/L, PS = 20.52 mM)

removal efficiency. In such circumstances, the removal efficiency for PS/nZVI, PS/Heat, and PS/Heat/nZVI systems was observed to be about 9, 94.5, and 98.4%, respectively. A number of similar results have been reported, which confirm our results (Cai et al. 2018; Zhou et al. 2018). The synergism among the PS, heat, and nZVI was determined using the pseudo-first-order degradation rate constants (*K*). Figure 9 b shows the coefficient (*K*) values for combined and separate processes. Based on Eq. (6), the synergy index (SI) was calculated by coefficient (*K*) values. As it is seen from Fig. 9 c, the SI values higher than zero indicate a synergistic effect between PS, heat, and nZVI.

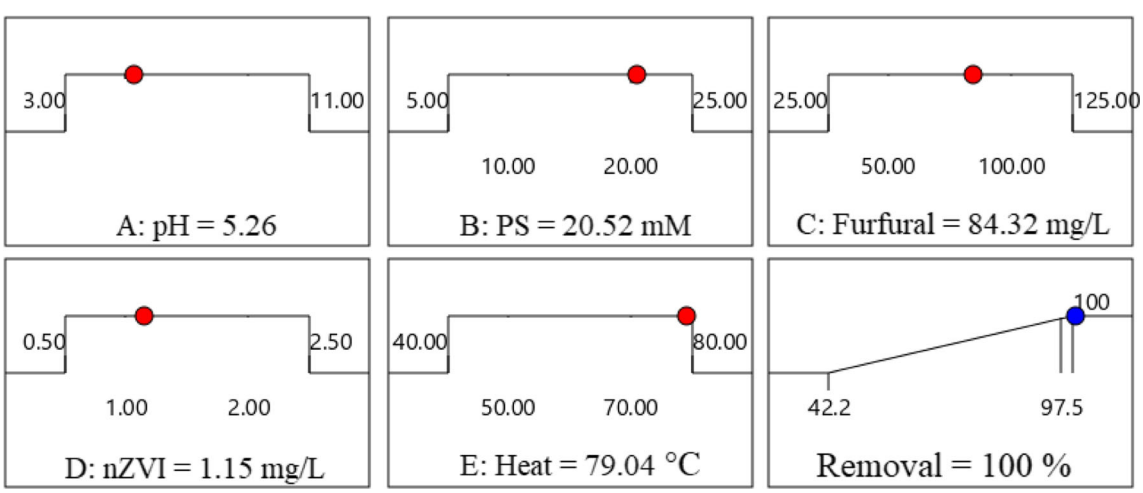

Fig. 8 The optimal conditions for the furfural removal in the TAP/nZVI process ($\alpha = \pm 2$)

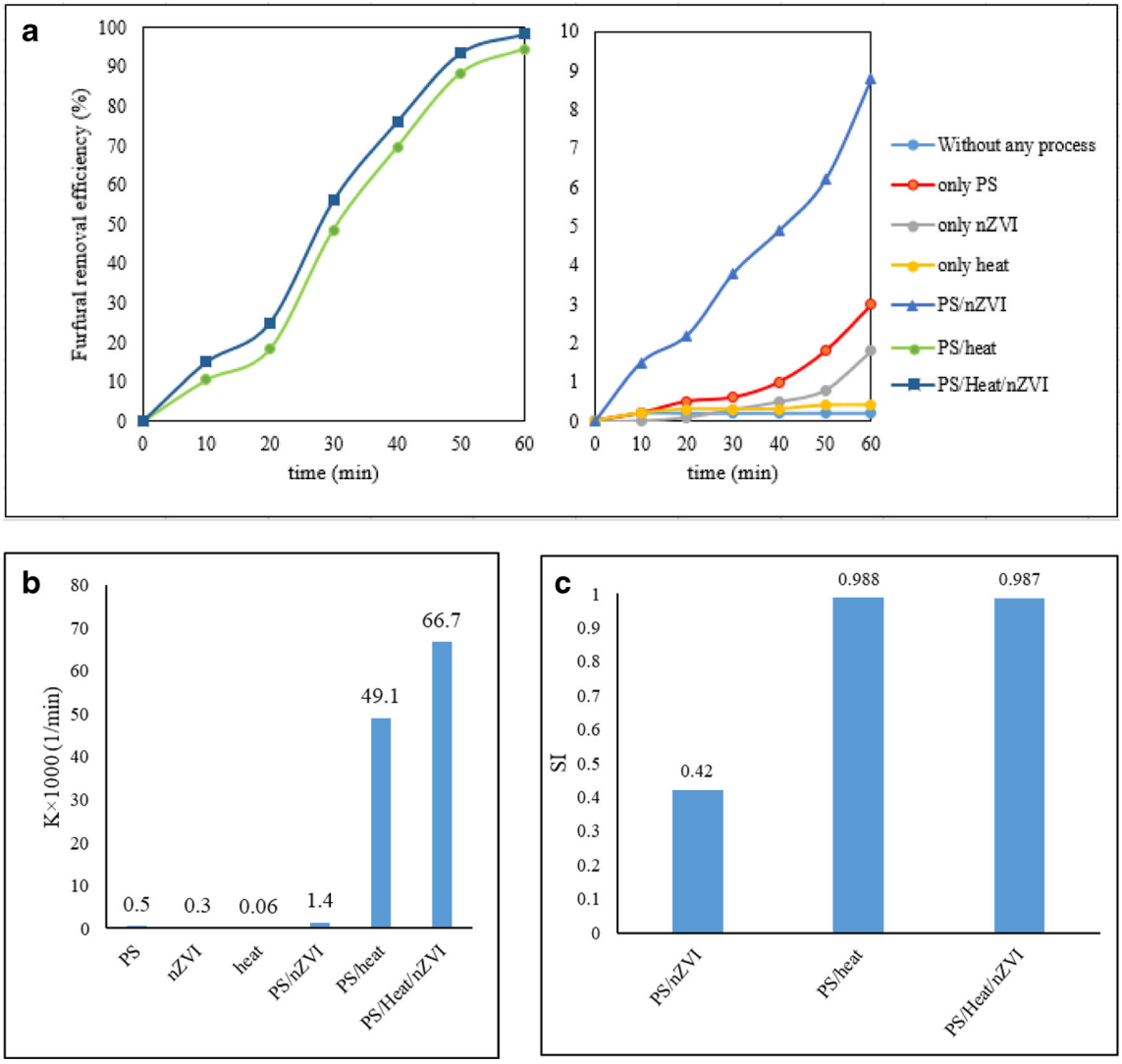

Fig. 9 Removal efficiency of furfural under different systems (**a**). The pseudo-first-order rate constants under different reaction system (**b**). The SI for hybrid processes (pH = 5.26, PS = 20.52 mM, furfural = 84.32 mg/L, nZVI = 1.15 mg/L, heat = 79 °C)

Furfural mineralization during TAP/nZVI oxidation process

Under the optimum conditions to confirm the furfural degradation, one sample was evaluated by monitoring the TOC removal rate, as shown in Fig. 10. The results showed that the TOC removal efficiency increased with reaction time increasing. So that, after 30- and 120-min operating time of the TAP/nZVI oxidation process, the TOC removal efficiency was observed to be 12.5 and 86.4%, respectively. These results showed furfural was degraded into its intermediate components that are not CO_2 and H_2O (Veisi et al. 2016). It is worth mentioning the decrease of TOC removal rate within 90 to 120 min indicates that the produced intermediates are resistant to degradation at present condition (Nezamzadeh-Ejhieh and Moeinirad 2011).

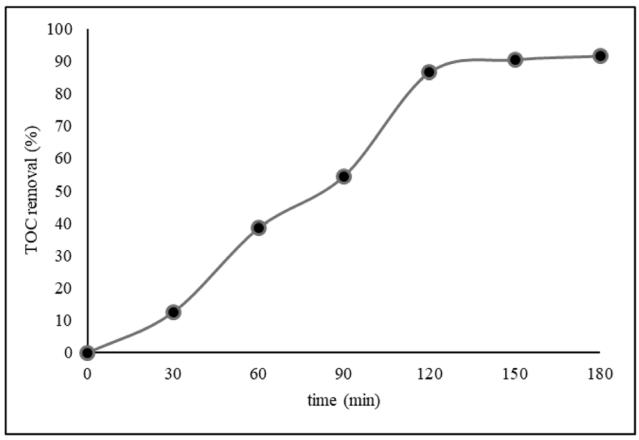

Fig. 10 Furfural mineralization during TAP/nZVI oxidation process. (pH = 5.26, PS = 20.52 mM, pH = 4.84, furfural = 84.32 mg/L, nZVI = 1.15 mg/L, heat = 79 °C)

Conclusion

In this study, thermochemical degradation of furfural was investigated using TAP/nZVI oxidation process, and the five independent variables were optimized by RSM based on CCD. The validity and accuracy of the obtained quadratic model was confirmed by a high R^2 coefficient ($R^2 = 0.975$). The Pareto analysis confirmed that the heat was the most effective operational parameter with 89.2% effect. The furfural removal efficiency at optimum conditions for the TAP/nZVI, TAP, PS/nZVI, non-activated PS, and nZVI was obtained as 98.4, 94.5, 9, 3, and 2%, respectively, which confirms the synergistic effect for the combined process. This study illustrated that the TAP process is a promising method for the removal of furfural in aqueous solution, as well as RSM-CCD, can be a beneficial tool to identify the most effective operating parameter and to optimize of the process. However, real applications of this procedure under typical treatment conditions should be further investigated in various aspects, for instance, technical and engineering studies for the feasibility of implementing this process on a practical scale, and further studies to investigate the effect of inhibitors and the application of the process in a complex natural matrix, economic studies to estimate the cost of construction and operation, and ecotoxicological analysis to assess the toxicity of products derived from furfural degradation.

Acknowledgments The authors appreciate the supports from the Hamadan University of Medical Sciences of Iran.

References

Abdessalem AK, Oturan N, Bellakhal N, Dachraoui M, Oturan MA (2008) Experimental design methodology applied to electro-Fenton treatment for degradation of herbicide chlortoluron. Appl Catal B Environ 78:334–341

Anupam K, Dutta S, Bhattacharjee C, Datta S (2011) Adsorptive removal of chromium (VI) from aqueous solution over powdered activated carbon: optimisation through response surface methodology. Chem Eng J 173:135–143

Asfaram A, Ghaedi M, Ghezelbash GR, Dil EA, Tyagi I, Agarwal S, Gupta VK (2016) Biosorption of malachite green by novel biosorbent Yarrowia lipolytica isf7: application of response surface methodology. J Mol Liq 214:249–258

Babuponnusami A, Muthukumar K (2012) Removal of phenol by heterogenous photo electro Fenton-like process using nano-zero valent iron. Sep Purif Technol 98:130–135

Borghei SM, Hosseini SN (2008) Comparison of furfural degradation by different photooxidation methods. Chem Eng J 139:482–488

Cai J, Zhou M, Yang W, Pan Y, Lu X, Serrano KG (2018) Degradation and mechanism of 2,4-dichlorophenoxyacetic acid (2,4-D) by thermally activated persulfate oxidation. Chemosphere 212:784–793

Chakma S, Praneeth S, Moholkar VS (2017) Mechanistic investigations in sono-hybrid (ultrasound/Fe2+/UVC) techniques of persulfate activation for degradation of Azorubine. Ultrason Sonochem 38:652–663

Chen X, Murugananthan M, Zhang Y (2016) Degradation of p-Nitrophenol by thermally activated persulfate in soil system. Chem Eng J 283:1357–1365

Cho I-H, Zoh K-D (2007) Photocatalytic degradation of azo dye (reactive red 120) in TiO2/UV system: optimization and modeling using a response surface methodology (RSM) based on the central composite design. Dyes Pigments 75:533–543

Cuevas M, Quero SM, Hodaifa G, López AJM, Sánchez S (2014) Furfural removal from liquid effluents by adsorption onto commercial activated carbon in a batch heterogeneous reactor. Ecol Eng 68:241–250

Deng J, Shao Y, Gao N, Deng Y, Zhou S, Hu X (2013) Thermally activated persulfate (TAP) oxidation of antiepileptic drug carbamazepine in water. Chem Eng J 228:765–771

Dong H, He Q, Zeng G, Tang L, Zhang L, Xie Y, Zeng Y, Zhao F (2017) Degradation of trichloroethene by nanoscale zero-valent iron (nZVI) and nZVI activated persulfate in the absence and presence of EDTA. Chem Eng J 316:410–418

Durán A, Monteagudo JM, Expósito AJ, Monsalve V (2016) Modeling the sonophoto-degradation/mineralization of carbamazepine in aqueous solution. Chem Eng J 284:503–512

Eslami A, Asadi A, Meserghani M, Bahrami H (2016) Optimization of sonochemical degradation of amoxicillin by sulfate radicals in aqueous solution using response surface methodology (RSM). J Mol Liq 222:739–744

Faramarzpour M, Vossoughi M, Borghei M (2009) Photocatalytic degradation of furfural by titania nanoparticles in a floating-bed photoreactor. Chem Eng J 146:79–85

Ferkous H, Merouani S, Hamdaoui O, Pétrier C (2017) Persulfate-enhanced sonochemical degradation of naphthol blue black in water: evidence of sulfate radical formation. Ultrason Sonochem 34:580–587

Frontistis Z, Antonopoulou M, Konstantinou I, Mantzavinos D (2017) Degradation of ethyl paraben by heat-activated persulfate oxidation: statistical evaluation of operating factors and transformation pathways. Environ Sci Pollut Res 24:1073–1084

Gao Y-Q, Gao N-Y, Deng Y, Yin D-Q, Zhang Y-S, Rong W-L, Zhou S-D (2015) Heat-activated persulfate oxidation of sulfamethoxazole in water. Desalin Water Treat 56:2225–2233

Gao Y-Q, Gao N-Y, Wang W, Kang S-F, Xu J-H, Xiang H-M, Yin D-Q (2018) Ultrasound-assisted heterogeneous activation of persulfate by nano zero-valent iron (nZVI) for the propranolol degradation in water. Ultrason Sonochem 49:33–40

George C, Rassy HE, Chovelon JM (2001) Reactivity of selected volatile organic compounds (VOCs) toward the sulfate radical (SO4−). In J Chem Kinet 33:539–547

Ghafari S, Aziz HA, Isa MH, Zinatizadeh AA (2009) Application of response surface methodology (RSM) to optimize coagulation–flocculation treatment of leachate using poly-aluminum chloride (PAC) and alum. J Hazard Mater 163:650–656

Ghauch A, Tuqan AM, Kibbi N (2012) Ibuprofen removal by heated persulfate in aqueous solution: a kinetics study. Chem Eng J 197:483–492

Hazime R, Nguyen QH, Ferronato C, Huynh TKX, Jaber F, Chovelon JM (2013) Optimization of imazalil removal in the system UV/TiO2/K2S2O8 using a response surface methodology (RSM). Appl Catal B Environ 132:519–526

He Y, Pei M, Du Y, Yu F, Wang L, Guo W (2014) Synthesis, characterization and application of chitosan coated Fe3O4 particles as an adsorbent for the removal of furfural from aqueous solution. RSC Adv 4:30352–30357

Hu P, Long M (2016) Cobalt-catalyzed sulfate radical-based advanced oxidation: A review on heterogeneous catalysts and applications. Appl Catal B Environ 181:103–117

Huang K-C, Couttenye RA, Hoag GE (2002) Kinetics of heat-assisted persulfate oxidation of methyl tert-butyl ether (MTBE). Chemosphere 49:413–420

Hussain I, Zhang Y, Huang S, Du X (2012) Degradation of p-chloroaniline by persulfate activated with zero-valent iron. Chem Eng J 203:269–276

Jafarinejad S (2017) Activated sludge combined with powdered activated carbon (PACT process) for the petroleum industry wastewater treatment: a review. Chem Int 3:268–277

Ji Y, Fan Y, Liu K, Kong D, Lu J (2015) Thermo activated persulfate oxidation of antibiotic sulfamethoxazole and structurally related compounds. Water Res 87:1–9

Ji Y, Xie W, Fan Y, Shi Y, Kong D, Lu J (2016) Degradation of trimethoprim by thermo-activated persulfate oxidation: reaction kinetics and transformation mechanisms. Chem Eng J 286:16–24

Khan S, He X, Khan JA, Khan HM, Boccelli DL, Dionysiou DD (2017) Kinetics and mechanism of sulfate radical-and hydroxyl radical-induced degradation of highly chlorinated pesticide lindane in UV/peroxymonosulfate system. Chem Eng J 318:135–142

Lau TK, Chu W, Graham NJ (2007) The aqueous degradation of butylated hydroxyanisole by UV/S2O82-: study of reaction mechanisms via dimerization and mineralization. Environ Sci Technol 41:613–619

Li R, Cai M, Liu H, Liu G, Lv W (2018) Thermo-activated peroxydisulfate oxidation of indomethacin: kinetics study and influences of co-existing substances. Chemosphere 212:1067–1075

Liang C, Su H-W (2009) Identification of sulfate and hydroxyl radicals in thermally activated persulfate. Ind Eng Chem Res 48:5558–5562

Lin Y-T, Liang C, Chen J-H (2011) Feasibility study of ultraviolet activated persulfate oxidation of phenol. Chemosphere 82:1168–1172

Liu A, Liu J, W-x Z (2015) Transformation and composition evolution of nanoscale zero valent iron (nZVI) synthesized by borohydride reduction in static water. Chemosphere 119:1068–1074

Liu L, Lin S, Zhang W, Farooq U, Shen G, Hu S (2018) Kinetic and mechanistic investigations of the degradation of sulfachloropyridazine in heat-activated persulfate oxidation process. Chem Eng J 346:515–524

Lucas S, Cocero MJ, Zetzl C, Brunner G (2004) Adsorption isotherms for ethylacetate and furfural on activated carbon from supercritical carbon dioxide. Fluid Phase Equilib 219:171–179

Moghaddam SS, Moghaddam MA, Arami M (2010) Coagulation/flocculation process for dye removal using sludge from water treatment plant: optimization through response surface methodology. J Hazard Mater 175:651–657

Moradi M, Ghanbari F (2014) Application of response surface method for coagulation process in leachate treatment as pretreatment for Fenton process: biodegradability improvement. J Water Process Eng 4:67–73

Moradi M, Ghanbari F, Manshouri M, Angali KA (2016) Photocatalytic degradation of azo dye using nano-ZrO2/UV/persulfate: response surface modeling and optimization. Korean J Chem Eng 33:539–546

Nezamzadeh-Ejhieh A, Moeinirad S (2011) Heterogeneous photocatalytic degradation of furfural using NiS-clinoptilolite zeolite. Desalination 273:248–257

Nie M, Yang Y, Zhang Z, Yan C, Wang X, Li H, Dong W (2014) Degradation of chloramphenicol by thermally activated persulfate in aqueous solution. Chem Eng J 246:373–382

Norzaee S, Taghavi M, Djahed B, Kord Mostafapour F (2018) Degradation of penicillin G by heat activated persulfate in aqueous solution. J Environ Manag 215:316–323

Oh S-Y, Kim H-W, Park J-M, Park H-S, Yoon C (2009) Oxidation of polyvinyl alcohol by persulfate activated with heat, Fe 2+, and zero-valent iron. J Hazard Mater 168:346–351

Olmez-Hanci T, Arslan-Alaton I (2013) Comparison of sulfate and hydroxyl radical based advanced oxidation of phenol. Chem Eng J 224:10–16

Priya, Kaith BS, Shanker U, Gupta B, Bhatia JK (2018) RSM-CCD optimized in-air synthesis of photocatalytic nanocomposite: application in removal-degradation of toxic brilliant blue. React Funct Polym 131:107–122

Purkait MK, Maiti A, Dasgupta S, De S (2007) Removal of congo red using activated carbon and its regeneration. J Hazard Mater 145: 287–295

Qian Y, Xue G, Chen J, Luo J, Zhou X, Gao P, Wang Q (2018) Oxidation of cefalexin by thermally activated persulfate: kinetics, products, and antibacterial activity change. J Hazard Mater 354:153–160

Rahmani AR, Rezaeivahidian H, Almasi M, Shabanlo A, Almasi H (2016) A comparative study on the removal of phenol from aqueous solutions by electro–Fenton and electro–persulfate processes using iron electrodes. Res Chem Intermed 42:1441–1450

Rahmani AR, Shabanloo A, Fazlzadeh M, Poureshgh Y, Rezaeivahidian H (2017) Degradation of acid blue 113 in aqueous solutions by the electrochemical advanced oxidation in the presence of persulfate. Desalin Water Treat 59:202–209

Rani SK, Easwaramoorthy D, Bilal IM, Palanichamy M (2009) Studies on Mn (II)-catalyzed oxidation of α-amino acids by peroxomonosulphate in alkaline medium-deamination and decarboxylation: a kinetic approach. Appl Catal A Gen 369:1–7

Sahu AK, Mall ID, Srivastava VC (2007) Studies on the adsorption of furfural from aqueous solution onto low-cost bagasse fly ash. Chem Eng Commun 195:316–335

Sahu AK, Srivastava VC, Mall ID, Lataye DH (2008) Adsorption of furfural from aqueous solution onto activated carbon: kinetic, equilibrium and thermodynamic study. Sep Sci Technol 43:1239–1259

Seid-Mohammadi A, Shabanloo A, Fazlzadeh M, Poureshgh Y (2017) Degradation of acid blue 113 by US/H2O2/Fe2+ and US/S2O8 2–/Fe2+ processes from aqueous solutions. Desalin Water Treat 78: 273–280

Sharma J, Anand P, Pruthi V, Chaddha AS, Bhatia J, Kaith B (2017) RSM-CCD optimized adsorbent for the sequestration of carcinogenic rhodamine-B: kinetics and equilibrium studies. Mater Chem Phys 196:270–283

Singh S, Srivastava VC, Mall ID (2009) Fixed-bed study for adsorptive removal of furfural by activated carbon. Colloids Surf A Physicochem Eng Asp 332:50–56

Song H, Yan L, Jiang J, Ma J, Zhang Z, Zhang J, Liu P, Yang T (2018) Electrochemical activation of persulfates at BDD anode: radical or nonradical oxidation? Water Res 128:393–401

Tan C, Gao N, Deng Y, Li L, Deng J, Zhou S (2015) Kinetic oxidation of antipyrine in heat-activated persulfate. Desalin Water Treat 53:263–271

Veisi F, Zazouli MA, Ebrahimzadeh MA, Charati JY, Dezfoli AS (2016) Photocatalytic degradation of furfural in aqueous solution by N-doped titanium dioxide nanoparticles. Environ Sci Pollut Res 23: 21846–21860

Vilardi G, Sebastiani D, Miliziano S, Verdone N, Di Palma L (2018) Heterogeneous nZVI-induced Fenton oxidation process to enhance biodegradability of excavation by-products. Chem Eng J 335:309–320

Wang X, Wang L, Li J, Qiu J, Cai C, Zhang H (2014) Degradation of acid orange 7 by persulfate activated with zero valent iron in the presence of ultrasonic irradiation. Sep Purif Technol 122:41–46

Wang T, Meng Y, Qin Y, Feng W, Wang C (2018a) Removal of furfural and HMF from monosaccharides by nanofiltration and reverse osmosis membranes. J Energy Inst 91:473–480

Wang Z, Shao Y, Gao N, Lu X, An N (2018b) Degradation kinetic of phthalate esters and the formation of brominated byproducts in heat-activated persulfate system. Chem Eng J

Wei L-L, Chen W-M, Li Q-B, Gu Z-P, Zhang A-P (2018) Treatment of dinitrodiazophenol industrial wastewater in heat-activated persulfate system. RSC Adv 8:20603–20611

Wirtz RA, Dague RR (1993) Anaerobic treatment of a furfural-production wastewater. Waste Manag 13:309–315

Yehia FZ, Eshaq G, Rabie AM, Mady AH, ElMetwally AE (2015) Phenol degradation by advanced Fenton process in combination with ultrasonic irradiation. Egypt J Pet 24:13–18

Zarei AR, Rezaeivahidian H, Soleymani AR (2015) Investigation on removal of p-nitrophenol using a hybridized photo-thermal activated persulfate process: central composite design modeling. Process Saf Environ Prot 98:109–115

Zeitsch KJ (2000) The chemistry and technology of furfural and its many by-products. Sugar series, vol 13. Elsevier, Amsterdam

Zhang D, Ong YL, Li Z, Wu JC (2013) Biological detoxification of furfural and 5-hydroxyl methyl furfural in hydrolysate of oil palm empty fruit bunch by Enterobacter sp. FDS8. Biochem Eng J 72:77–82

Zhao L, Hou H, Fujii A, Hosomi M, Li F (2014) Degradation of 1,4-dioxane in water with heat- and Fe2+-activated persulfate oxidation. Environ Sci Pollut Res 21:7457–7465

Zhou R, Li T, Su Y, Ma T, Zhang L, Ren H (2018) Oxidative removal of metronidazole from aqueous solution by thermally activated persulfate process: kinetics and mechanisms. Environ Sci Pollut Res 25: 2466–2475